Structural and Spectroscopic Studies of Two Phases of the Organometallic Chain Polymer $[Ru_2\{\mu_2{:}\mu_2{:}\eta^2\text{-}O_2PMe_2\}_2(CO)_4]_n$

Christopher M. Barnes,[†] D. Scott Bohle,*[,†] Robert E. Dinnebier,*[,‡,§] Sara K. Madsen,[†] and Peter W. Stephens[‡]

Department of Chemistry, University of Wyoming, Laramie, Wyoming 82071-3838, and Department of Physics, State University of New York, Stony Brook, New York, 11794

Received March 5, 1997[⊗]

The microcrystalline organometallic coordination polymer $[Ru_2\{\mu_2{:}\mu_2{:}\eta^2\text{-}O_2PMe_2\}_2(CO)_4]_n$ which results from the oxidative addition of dimethylphosphinic acid to triruthenium dodecacarbonyl has been structurally characterized by X-ray powder diffraction, $\lambda = 1.149\ 49(1)$ Å, at 295 and 50 K. At room temperature the crystallites have a monoclinic unit cell with the space group $C2/c$ with lattice constants $a = 18.0792(3)$ Å, $b = 9.0626(2)$ Å, $c = 10.0372(2)$ Å, $\beta = 112.107(1)°$, and $Z = 4$; the final refinement of 52 variables converged to R_p, R_{wp}, R_F, and R_{F^2} of 8.2, 10.8, 4.6, and 8.3%, respectively, for data collected between 4 and 60° (2θ). At 50 K the phase is described by a triclinic unit cell, space group $P\bar{1}$, and is characterized by the lattice constants $a = 9.8637(6)$ Å, $b = 8.9290(6)$ Å, $c = 9.8870(5)$ Å, $\alpha = 115.051(3)°$, $\beta = 108.587(5)°$, $\gamma = 92.015(5)°$, and $Z = 2$; the final refinement of 102 variables converged to and R_p, R_{wp}, R_F, and R_{F^2} of 8.3, 11.4, 1.5, and 3.0%, respectively, for data collected between 3 and 74° (2θ). The transition between the two crystalline phases has been determined by differential scanning calorimetry to occur at circa 220 K, and the most pronounced difference in the environment of the chains, as determined by variable-temperature IR spectroscopy, is in the $\rho(PCH_3)$ modes for the bridging dimethylphosphinate ligands.

Introduction

The oxidative addition reactions of low-valent transition metal compounds frequently results in the formation of insoluble microcrystalline organometallic polymers. While there is an extensive derivative chemistry of these species,[1] and many are useful reagents and catalyst precursors,[2] their structures are often unknown due to the general inability to obtain suitable crystals for conventional single-crystal X-ray diffraction. However, structural characterization by powder diffraction techniques is able to solve increasingly difficult problems and there is growing recognition of its utility in all avenues of inorganic chemistry.[3] We describe here the spectroscopic and structural characterization of two phases for one such organometallic polymer, $[Ru_2\{\mu_2{:}\mu_2{:}\eta^2\text{-}O_2PMe_2\}_2(CO)_4]_n$, as determined by IR spectroscopy and X-ray powder diffraction. The diffraction results indicate that an unusual distortion occurs within the chain-propagating interaction during a phase transition near 220 K.

Results and Discussion

Thin needlelike crystals of $[Ru_2\{\mu_2{:}\mu_2{:}\eta^2\text{-}O_2PMe_2\}_2(CO)_4]_n$, **1**, form when $Ru_3(CO)_{12}$ is treated with dimethylphosphinic acid in tetrahydrofuran at 50°C, eq 1.[4] The product has been

$$2Ru_3(CO)_{12} + 6Me_2PO_2H \xrightarrow{THF,\ \Delta} [Ru_2(\mu_2;\mu_2;\eta^2\text{-}O_2PMe_2)_2(CO)_4]_n + 12\,CO + 3\,H_2 \quad (1)$$

1

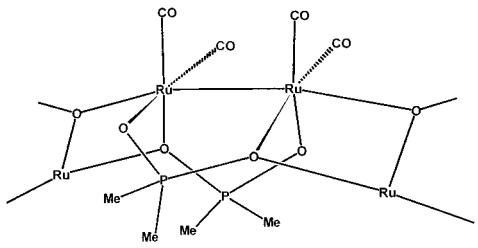

1

formulated as a dimer of ruthenium(I) centers on the basis of its elemental analysis, IR spectroscopy, and derivative chemistry. A broad range of carboxylate-bridged analogues have been prepared by the oxidative addition of carboxylic acids to $Ru_3(CO)_{12}$ under forcing conditions, *e.g.* acetic acid at reflux.[2] In one case diffraction-quality single crystals of the benzoate-bridged polymer, $[Ru_2\{\mu_2{:}\mu_2{:}\eta^2\text{-}O_2CPh\}_2(CO)_4]_n$, have been

[†] University of Wyoming.
[‡] SUNY at Stony Brook.
[§] Current address: Laboratory of Crystallography, University of Bayreuth, D-95440 Bayreuth, Germany.
[⊗] Abstract published in *Advance ACS Abstracts,* November 1, 1997.

(1) See, for example, various chapters of: *Comprehensive Organometallic Chemistry*; Wilkinson, Stone, and Abel, Eds.; Pergamon Press: Oxford, U.K., 1982.
(2) (a) Bright, T. A.; Jones, R. A.; Nunn, C. M. *J. Coord. Chem.* **1988**, *18*, 361. (b) Bianchi, M.; Matteoli, U.; Frediani, P; Piacenti, F; Mardelli, M.; Pelizzi, G. *Chim. Ind. (Milan)* **1981**, *63*, 475. (c) Bulllitt, J. G.; Cotton, F. A. *Inorg. Chim. Acta* **1971**, *5*, 406. (d) Bianchi, M.; Frediani, P.; Mardelli, M.; Pelizzi, G. *Acta Crystallogr. A* **1981**, *37*, C236. (e) Rotem, M.; Goldberg, I.; Shmueli, U.; Shvo, Y. *J. Organomet. Chem.* **1986**, *314*, 185. (f) Rotem, M.; Shvo, Y.; Goldberg, I.; Shmueli, U. *Organometallics* **1984**, *3*, 1758. (g) Rotem, M.; Goldberg, I.; Shvo, Y. *Inorg. Chim. Acta* **1985**, *97*, L27. (h) Schumann, H.; Opitz, J.; Pickardt, J. *J. Organomet. Chem.* **1977**, *128*, 253. (I) Süss-Fink, G.; Wolfender, L.-L.; Neumann, F.; Stoeckli-Evans, H. *Angew. Chem., Int. Ed. Engl.* **1990**, *29*, 429. (j) Sherlock, S. J.; Cowie, M.; Singleton, E.; de V. Steyn, M. M. *Organometallics* **1988**, *7*, 1663. (k) Hilts, R. W.; Sherlock, S. J.; Cowie, M; Singleton, E.; de V. Steyn, M. M. *Inorg. Chem.* **1990**, *29*, 3161.
(3) (a) Masciocchi, N.; Moret, M.; Cairati, P.; Ragaini, F.; Sironi, A. *J. Chem. Soc., Dalton Trans.* **1993**, 471. (b) Masciocchi, N.; Cairati, P.; Ragaini, F.; Sironi, A. *Organometallics* **1993**, *12*, 4499. (c) Poojary, D. M.; Zhang, B.; Clearfield, A.; *Angew. Chem., Int. Ed. Engl.* **1994**, *33*, 2325. (d) Masciocchi, N.; Moret, M.; Cairati, P.; Sironi, A.; Ardizzoia, G. A.; La Monica, G. *J. Am. Chem. Soc.* **1994**, *116*, 7668. Dinnebier, R. E.; Pink, M.; Sieler, J.; Stephens, P. W. *Inorg. Chem.*, in press.
(4) Barnes, C. M.; Bohle, D. S.; Madsen, S. K. *Inorg. Chem.* **1994,** *33*, 6411.

S0020-1669(97)00265-6 CCC: $14.00

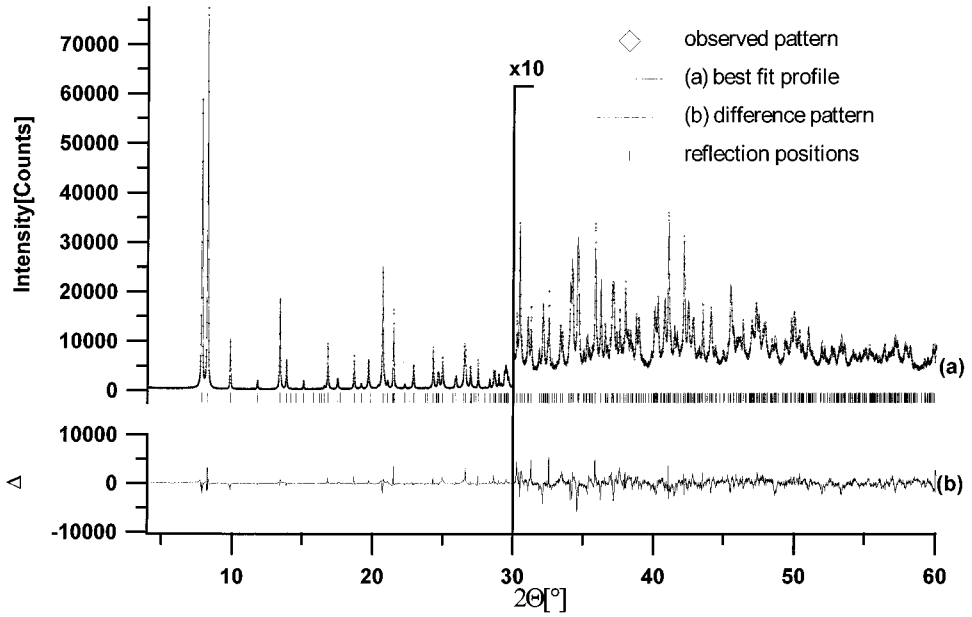

Figure 1. Rietveld plot of the powder diffraction pattern for $[Ru_2(\mu_2{:}\mu_2{:}\eta^2\text{-}O_2PMe_2)(CO)_4]_n$ at 295 K. The observed pattern (dots), the best fit (solid line), and the difference curve are given. Tick marks show the allowed peak positions. Note the change of scale at 30° in 2θ (b). See the Experimental Section for complete collection details.

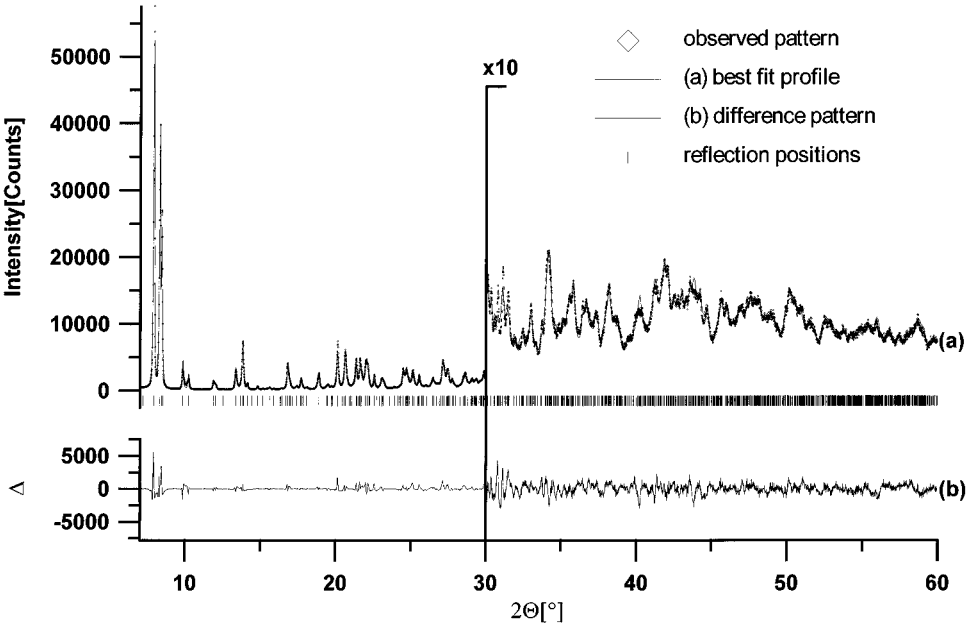

Figure 2. Rietveld plot of the powder diffraction pattern for $[Ru_2(\mu_2{:}\mu_2{:}\eta^2\text{-}O_2PMe_2)(CO)_4]_n$ at 50 K. Note the change of scale at 30° in 2θ. The plot conventions and symbols are the same as in Figure 1.

prepared from a benzoic acid melt in a sealed tube.[5] Similar preparations of **1** from neat melts of dimethylphosphinic acid, mp = 87 °C, return dark insoluble materials of low purity; attempts to prepare **1** by means which would result in larger crystals suitable for single-crystal X-ray diffraction have so far failed. Nevertheless, the microcrystals of **1** from the solution preparation shown in eq 1 have a sharp, well-resolved diffraction pattern out to $\sin(\theta)/\lambda = 0.43$ Å^{-1} at room temperature, Figure 1. Upon cooling to 50 K, this material undergoes a phase transition to a less symmetric material which gives the diffraction pattern of significantly lower resolution shown in Figure 2.

The structures of both of these phases have been solved from powder data by a combination of direct methods and restricted grid search techniques and refined by Rietveld least-squares fitting to give the final parameters and fits shown in Table 1 and Figures 1 and 2. Both phases share a common bisphosphinate ruthenium−ruthenium bonded dimer fragment which is oligomerized into a strand by interdimer ruthenium−oxygen bonds. Views of these strands are shown in Figures 3 and 4 for the room-temperature and low-temperature phases. Metrical parameters are collected in Tables 2−5, and atomic positional parameters have been deposited as Supporting Information.

Although the structures of the low- and room-temperature phases of **1** are similar, there are subtle changes in geometry, *i.e.* the torsion angles, τ, around the ruthenium−ruthenium bonds within the phosphinate bridges, are smaller for the low-temperature phase than for the room-temperature phase, which has a single unique τ of 10.1° for O1−Ru1−Ru1A−O2. These torsion angles are substantially less than those found for the phosphinate-bridged dimers $[Ru_2\{\eta^2{:}\mu_2\text{-}O_2PR_2\}_2(CO)_4(PPh_3)_2]$ where R = Me, τ = 26.1°, and R = Ph, τ = 22.0°, but are

(5) Spohn, M.; Vogt, T.; Strähle, J. *Z. Naturforsch., B* **1986**, *41*, 1373.

Table 1. Crystallographic Parameters for $[Ru_2\{\mu_2{:}\mu_2{:}\eta^2\text{-}O_2PMe_2\}_2(CO)_4]_n$, **1**

temp (K)	295	50
2θ range (deg)	4.00−60.0	3.00−74.0
a (Å)	18.0792(3)	9.8637(6)
b (Å)	9.0626(2)	8.9290(6)
c (Å)	10.0372(1)	9.8870(5)
α (deg)	90	115.051(3)
β (deg)	112.107(1)	108.587(5)
γ (deg)	90	92.015(5)
V (Å^3)	1523.64(5)	732.9(8)
Z	4	2
formula	$C_8H_6O_8P_2Ru_2$	$C_8H_6O_8P_2Ru_2$
space group	$C2/c$	$P\bar{1}$
D_{exp} (g cm^{-3})	2.17(1)	
D_{calc} (g cm^{-3})	2.154	2.24
refined variables	52	102
R_p	0.082	0.083
R_{wp}	0.108	0.114
R_F, R_{F^2}	0.046, 0.083	0.015, 0.030

[a] Data collected with monochromatic X-rays (λ = 1.149 49 Å) on a $\theta-2\theta$ scanning diffractometer with a flatplate geometry on beamline X3B1 at the National Synchrotron Light Source at the Brookhaven National Laboratories.

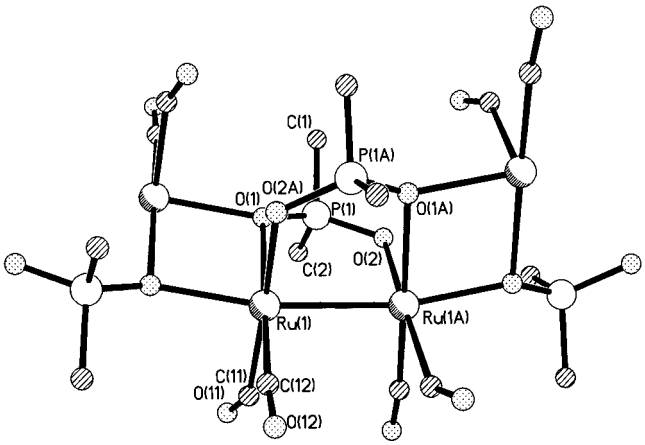

Figure 3. Side on view of chain present in the 295 K phase of $[Ru_2(\mu_2{:}\mu_2{:}\eta^2\text{-}O_2PMe_2)(CO)_4]_n$. Atom sizes are arbitrary. In addition to the asymmetric unit, enough symmetry-generated atoms are shown to describe both the dimeric structure and the chain propagation along the c-axis. Note the C_2 axis located at the center of the Ru−Ru bond.

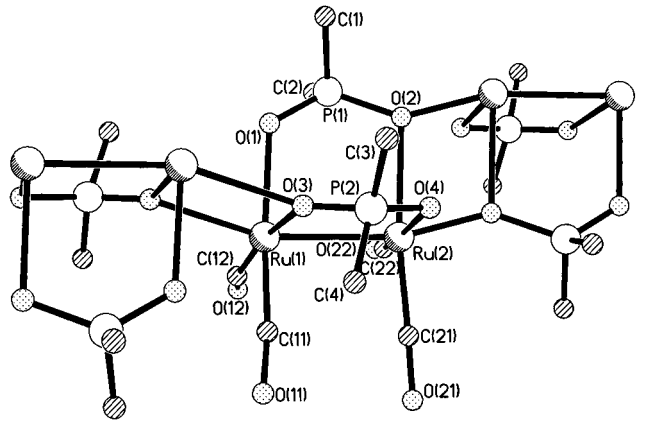

Figure 4. Side on view of the chain present in the 50 K phase of $[Ru_2(\mu_2{:}\mu_2{:}\eta^2\text{-}O_2PMe_2)(CO)_4]_n$. Atom sizes are arbitrary. In addition to the asymmetric unit, which in this phase is a complete dimer, two adjacent dimers along the a-axis are shown without the CO ligands for clarity.

similar to those frequently found for the carboxylate-bridged analogues.[2,4,5] Within the dimethylphosphinate series of complexes there is a rough correlation of τ around the metal−metal bond and the donor ability of the ligand *trans* to this bond. For strong donor ligands such as triphenylphosphine there is a greater twist around the ruthenium−ruthenium bond. Along with these changes in torsion angle there is also a slight increase in the ruthenium−ruthenium bond distance for the triphenylphosphine adducts, R = Me, Ru−Ru = 2.781(1) Å, and R = Ph, Ru−Ru = 2.815(1) Å, versus 2.752(1) Å for the room-temperature phase of **1**. In addition to these changes in the geometry at ruthenium, the interdimer arrangement undergoes substantial alteration upon the phase transition. Figure 5 shows the room-temperature chain (in **bold** face) where all four *inter*dimer Ru−O contacts are related by the C_2 axis of the $C2/c$ space group; *i.e.*, the low-temperature chain (*italic* face) lacks this symmetry element and the Ru−O contacts are related only by inversion symmetry.

Upon cooling, the transition from the $C2/c$ ambient temperature phase to the low-temperature $P\bar{1}$ phase is not accompanied by any major shifts in the ν(CO) region of the IR spectrum, Figure 6. Instead, we see peaks at almost the same positions but noticeably broader in the less symmetric phase; also, the lowest-energy band at 1908−1910 cm^{-1} is noticeably more intense in the low-temperature phase. These slight differences can be rationalized by the loss of geometric symmetry alone, since the transition dipole moment of symmetric stretches tends

Table 2. Bond Lengths (Å) in the Room-Temperature Phase of $[Ru_2\{\mu_2{:}\mu_2{:}\eta^2\text{-}O_2PMe_2\}_2(CO)_4]_n$[a]

Ru1−Ru1A	2.752(4)	Ru1−O1	2.474(1)
Ru1−C11	2.17(1)	Ru1−C12	2.08(1)
Ru1−O1A	2.23(9)	Ru1−O2A	2.24(1)
P1−O1	1.39(1)	P1−O2	1.53(1)
P1−C1	1.68(1)	P1−C2	1.65(2)
O11−C11	1.18(2)	O12−C12	1.17(1)

[a] Atoms labeled A are related by C_2 crystallographic symmetry to the original.

Table 3. Bond Angles (deg) for the Room-Temperature Phase of $[Ru_2\{\mu_2{:}\mu_2{:}\eta^2\text{-}O_2PMe_2\}_2(CO)_4]_n$[a]

O1−Ru1−C11	102(1)	O1−Ru1−C12	177(1)
O1−Ru1−Ru1A	86(1)	O1−Ru1−O2A	84(1)
O1−Ru1−O1B	84(1)	C11−Ru1−C12	80.3(6)
C11−Ru1−Ru1A	94(1)	C11−Ru1−O2A	173(1)
C11−Ru1−O1B	92(1)	C12−Ru1−Ru1A	94(1)
C12−Ru1−O2A	94(1)	C12−Ru1−O1B	96(1)
Ru1A−Ru1−O2A	89(1)	Ru1A−Ru1−O1B	169(1)
O2A−Ru1−O1B	85(1)	O1−P1−O2	122.4(9)
O1−P1−C1	103.3(9)	O1−P1−C2	108(1)
O2−P1−C1	111.5(9)	O2−P1−C2	108(1)
C1−P1−C2	102(1)	Ru1−O1−P1	116(2)
Ru1−O1−Ru1B	96(2)	P1−O1−Ru1B	145(2)
P1−O2−Ru1A	122(2)	Ru1−C11−O11	144(2)
Ru1−C12−O12	172(2)		

[a] Atoms labeled A and B are related by C_2 and i crystallographic symmetry, respectively, to the original.

Table 4. Bond Lengths (Å) in the Low-Temperature Phase of $[Ru_2\{\mu_2{:}\mu_2{:}\eta^2\text{-}O_2PMe_2\}_2(CO)_4]_n$[a]

Ru1−Ru2	2.748(7)	Ru1−O1	2.29(2)
Ru1−O3	2.36(2)	Ru1−O3A	2.40(2)
Ru1−C11	1.99(2)	Ru1−C12	1.92(2)
Ru2−O2	2.41(2)	Ru2−O2A	1.95(3)
Ru2−O4	2.29(2)	Ru2−C21	1.98(2)
Ru2−C22	1.98(2)	P1−O1	1.46(3)
P1−O2	1.60(2)	P1−C1	1.62(2)
P1−C2	1.49(2)	P2−O3	1.34(2)
P2−O4	1.53(2)	P2−C3	1.65(2)
P2−C4	1.56(2)	O11−C11	1.36(2)
O12−C12	1.32(2)	O21−C21	1.27(2)
O22−C22	1.20(2)		

[a] Atoms labeled A are related by i crystallographic symmetry to the original.

Table 5. Bond Angles (deg) for the Low-Temperature Phase of $[Ru_2\{\mu_2{:}\mu_2{:}\eta^2\text{-}O_2PMe_2\}_2(CO)_4]_n$[a]

Ru2−Ru1−O1	85.9(8)	Ru2−Ru1−O3	82(1)	Ru2−Ru1−C11	91(2)
Ru2−Ru1−C12	98(2)	Ru2−Ru1−O3A	162(1)	O1−Ru1−O3	84(2)
O1−Ru1−C11	174(2)	O1−Ru1−C12	107(2)	O1−Ru1−O3A	78(1)
O3−Ru1−C11	90(2)	O3−Ru1−C12	169(2)	O3−Ru1−O3A	88(1)
C11−Ru1−C12	79(2)	C11−Ru1−O3A	105(2)	C12−Ru1−O3A	94(2)
Ru1−Ru2−O2	92(1)	Ru1−Ru2−O4	90.3(8)	Ru1−Ru2−C21	93(1)
Ru1−Ru2−C22	95(1)	Ru1−Ru2−O2A	164(1)	O2−Ru2−O4	79(1)
O2−Ru2−C21	172(2)	O2−Ru2−C22	94(2)	O2−Ru2−O2A	74(2)
O4−Ru2−C21	96(2)	O4−Ru2−C22	171(2)	C21−Ru2−C22	91(2)
C21−Ru2−O2A	100(2)	C22−Ru2−O2A	93(2)	O1−P1−O2	123(2)
O1−P1−C1	101(2)	O1−P1−C2	104(2)	O2−P1−C1	105(2)
O2−P1−C2	110(2)	C1−P1−C2	115(2)	O3−P2−O4	118(2)
O3−P2−C3	109(2)	O3−P2−C4	91(3)	O4−P2−C3	108(2)
O4−P2−C4	120(2)	C3−P2−C4	109(2)	Ru1−O1−P1	124(2)
Ru2−O2−P1	108(2)	Ru2−O2−Ru2A	105(2)	P1−O2−Ru2A	143(2)
Ru1−O3−P2	127(2)	Ru1−O3−Ru1A	92(2)	P2−O3−Ru1A	127(2)
Ru2−O4−P2	118(2)	Ru1−C11−O11	159(4)	Ru2−C21−O21	172(4)
Ru1−C12−O12	159(4)	Ru2−C22−O22	174(5)		

[a] Atoms labeled A are related by *i* crystallographic symmetry to the original.

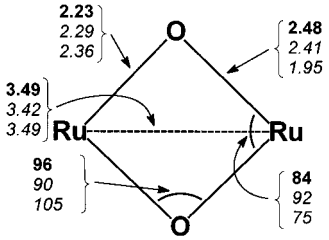

Figure 5. Scheme showing the changing geometry of the interdimer Ru−O contacts in the two phases. In bold font are distances and angles relating to the *C*2/*c* phase occurring at 295 K; below, in italics, are corresponding distances and angles in the *P*$\bar{1}$ phase found at 50 K.

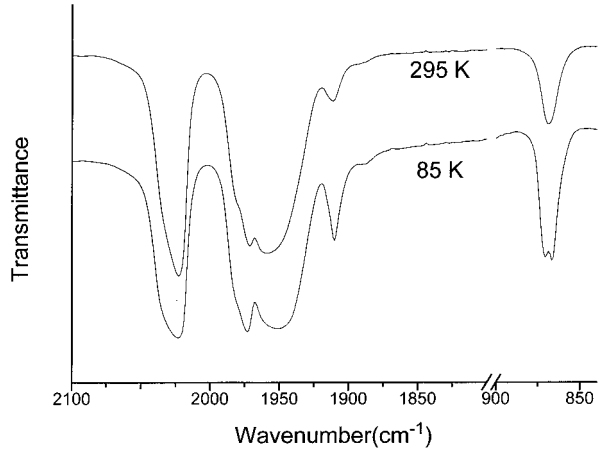

Figure 6. Room- and low-temperature IR spectra of $[Ru_2(\mu_2{:}\mu_2{:}\eta^2\text{-}O_2PMe_2)(CO)_4]_n$: (a) carbonyl stretching region; (b) lower-energy band we assign as the $P(Me)_2$ ρ-rock.

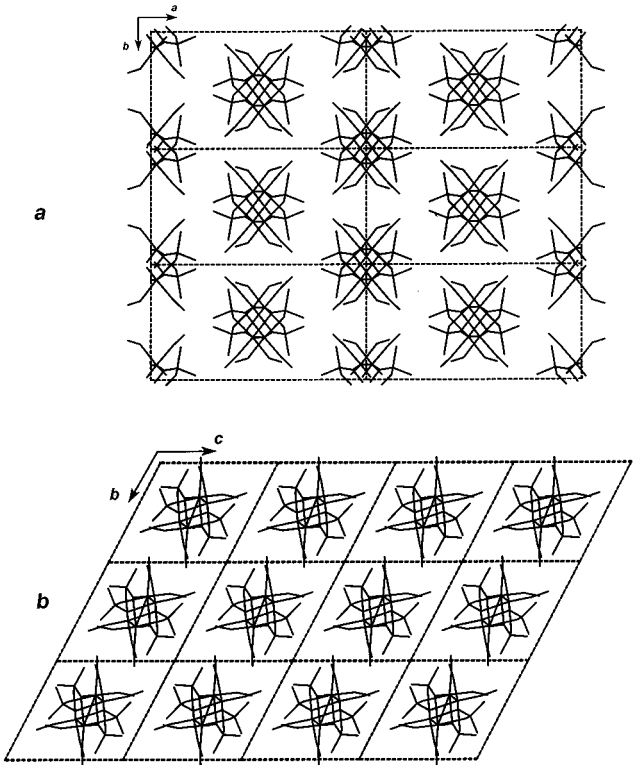

Figure 7. Packing diagrams for the high- (a) and low- (b) temperature phases for $[Ru_2(\mu_2{:}\mu_2{:}\eta^2\text{-}O_2PMe_2)(CO)_4]_n$. Both views are along the axis of chain propagation and show a stick representation of two dimeric units of the chain.

to increase upon a break in symmetry.[6] The IR data suggest that there is little change in the electronic environment of the ruthenium atoms upon the phase transition.

Despite the lack of gross changes in the ν(CO) IR data upon cooling, the lengths of the ruthenium−oxygen contacts differ significantly between the low-temperature and room-temperature structures. In the low-temperature phase the axial Ru2−O2A contact (which propagates the chain of oligimers) is the shortest of the six distinct Ru−O bond lengths defined by the structure. In the room-temperature phase the shortest Ru−O bond is internal to one dimer, as is the case for $[Ru_2\{\mu_2{:}\mu_2{:}\eta^2\text{-}O_2CPh\}_2(CO)_4]_n$.[5] We are reluctant to interpret the anomalous low-temperature result, especially since the ruthenium−ruthenium distances (which are the best-defined distances in the structure) do not show a related trend.

The structural changes that occur during the phase transition are most easily visualized with the aid of the packing diagrams shown in Figure 7 for the two phases. These views are depicted along the chain, which corresponds to the *a* axis for the low-temperature phase and the *c* axis for the room-temperature phase. In the room-temperature phase the carbonyl groups dominate the interchain interactions along the *b* axis where phosphinate methyl groups point toward each other along the diagonals of the cell. For the low-temperature phase this latter orientation is retained while the carbonyl groups become more staggered or interdigitated in the triclinic lattice. The energetics of this phase transformation are clearly a balance of the packing forces and the intrachain covalent interactions. The better packing of

(6) Nakamoto, K. *Infrared and Raman Spectra of Inorganic and Coordination Compounds*, 4th ed.; John Wiley and Sons: New York, 1986.

the low-temperature phase results in a more dense phase but at the cost of a somewhat unusual geometry for the phosphinate bridges. If this view is correct, one explanation then for the phase transition is that it is driven by the release of dimer ring strain at the cost of an expanded lattice with less dense packing.

Experimental Section

$[Ru_2\{\mu_2:\mu_2:\eta^2\text{-}O_2PMe_2\}_2(CO)_4]_n$ was prepared from dimethylphosphinic acid[7] and triruthenium dodecacarbonyl by literature methods.[4] This compound was handled without precautions against oxygen or moisture except where noted.

X-ray Powder Diffraction. High-resolution powder diffraction data were collected at the SUNY X3B1 beamline at the National Synchrotron Light Source, Brookhaven National Laboratory. X-rays of wavelength 1.149 49(1) Å were selected by a double Si(111) monochromator. The diffracted beam was analyzed with a Ge(111) crystal and detected with a Na(Tl)I scintillation counter with a pulse height discriminator in the counting chain. The incoming beam was monitored by an ion-chamber for normalization for the decay of the primary beam. In this parallel beam configuration, the resolution is determined by the analyzer crystal instead of by slits. For the powder X-ray diffraction experiments, the sample was side-loaded into a flat plate low-background quartz single crystal sample holder. Data were taken at room temperature for 3.2 s at each 2θ in steps of 0.01° from 4 to 60°. To decrease the thermal motion of the atoms and to evaluate the possibility of a distortion at low temperature, the sample was loaded in a flat plate brass sample holder and cooled to 50 K in a closed-cycle helium cryostat. From the pattern collected, a phase change was evident. Data were taken at 50 K for 10.2 s at each 2θ in steps of 0.01° from 3 to 74°. With a beam height $h = 2$ mm and a sample length $l = 16$ mm, the beam overspills the sample at low angles. We compensated for this effect by using a correction factor in the program GUFI[8] to multiply the measured intensity by the factor $h/(l \sin(2\theta/2))$ for $2\theta < 2 \sin^{-1} h/l = 14.4°$. No such correction was necessary for the room-temperature data because a longer sample holder was used.

Although θ-scans did not show serious crystallite size effects, the sample was rocked around θ by 3° at room temperature and 2° at low temperature throughout the experiment. Low-angle diffraction peaks had a fwhm of 0.042° in 2θ for the phase at room temperature and 0.061° in 2θ for the low-temperature phase. Both are significantly broader than the resolution of the spectrometer.

Indexing of the room-temperature phase with the Ito method[9] yielded a monoclinic lattice. The possible space groups (*C*2 and *C*2/*c*) and the number of formula units per unit cell (*Z*) were found by applying the extinction rules and geometrical considerations. A LeBail fit[10] using the program FULLPROF[11] worked well to extract about 160 integrated intensities up to a 2θ of 40°. These were used as input for the direct methods program SIRPOW92.[12] All attempts to find the structure in the centrosymmetric space group *C*2/*c* failed. After switching to the noncentrosymmetric group, it was possible to detect one complete wing of the dimer Ru−O−P−O−Ru and some fragment of the second wing. This information was sufficient to generate the complete molecule using chemical and geometrical considerations. Later refinements in both space groups were of equal quality, and we therefore switched back to *C*2/*c*.

We used the program package GSAS[13] for the final Rietveld[14] refinements, shown in Figures 1 and 2. The peak profile function was modeled using a multiterm Simpson's rule integration of the pseudo-Voigt function.[15] The strong asymmetry in the low-angle region was modeled by a recently implemented function[16] which accounts for the asymmetry due to axial divergence, leading to a strongly improved fit and therefore better profile *R*-factors. A manually fitted background was used in combination with a refinable four-term cosine series to give some flexibility back to the program. It was necessary to introduce soft constraints of Ru−Ru, P−O, C−O, and Ru−O distances to stabilize the refinement. The starting values for the bond lengths were taken from the reported single crystal structure of $Ru_2\{\mu_2:\eta^2\text{-}O_2PR_2\}_2(CO)_4(PPh_3)_2$, R = Ph, Me.[4]

The position of most of the atoms remained close to their original positions after turning all atoms loose in a final cycle of refinement, whereas the C atoms of the methyl groups and the O atoms of the CO groups tended to drift away further, albeit without improving the statistics of the fit. The *R*-values are listed in Table 1. The coordinates (using soft constraints) are given in the Supporting Information. A selection of metrical data is given in Tables 2 and 3.

Due to the lower symmetry the number of accidentally overlapping reflections in the powder pattern of the low-temperature structure strongly increased. At the same time the resolution of the powder pattern substantially decreased. Therefore it was impossible to resolve a sufficient number of individual reflection intensities and all attempts to solve the structure by direct methods failed.

Preliminary Rietveld fits[14] starting from arbitrary orientations were unsuccessful. For this reason, we attempted to find an approximate starting point by restricted grid searches of the fragment orientation. In such a search, it is not necessary to compare the entire profile; matching a number of selected integrated intensities is sufficient. About 40 relative intensities of adequately separated peaks and/or peak groups were extracted for simulation purposes.

Under the assumption that the shape of the Ru−O−P−O−Ru wings as the basic fragment of the structure remain essentially unchanged, the number of possible degrees of freedom can be dramatically reduced. Since it was not clear from the beginning that the structure preserves its center of symmetry, all preliminary calculations were carried out in *P*1. The direction of the polymeric chains could be found by comparison of the cell parameters of both phases. After the selection of one Ru atom as an arbitrary starting point, the length between identical Ru atoms (length of *a*-axis) can be divided into four Ru−Ru vectors whose individual lengths are known from the room-temperature structural solution. Evaluation of all possible rotations and movements results in a limited 6-dimensional grid search which lead to a usable starting model for Rietveld refinement. As in the case of the high-temperature structure, it was found that refinement in the centrosymmetric space group $P\bar{1}$ group was of equal quality, and so the remaining work was performed in that space group. The *R*-values are listed in Table 1. The coordinates are given in the Supporting Information. A selection of metrical data is given in Tables 4 and 5. Some differences between the observed and the calculated pattern can be assigned to the lack of H atoms in the model. Their position cannot be determined by powder techniques, but their contribution to the profile is definitely measurable.[17]

It should be noted that the quality of the refinement of the low-temperature structure is not as high as for the high-temperature phase, largely due to a more complicated background distribution. Although it was not possible to extract reasonable temperature factors for the individual atoms, their position could be determined precisely enough to justify the conclusions drawn in Results and Discussion.

Variable-Temperature IR. Samples were examined as KBr pellets in a liquid-nitrogen-cooled cell based on a previously reported design.[18] A Midac 101250-1-1 Fourier transform spectrometer was modified to accommodate the cooled cell. The sample cavity of the instrument

(7) Reinhardt, H.; Bianci, D.; Mölle, D. *Chem. Ber.* **1957**, *90*, 1656.
(8) Dinnebier, R. E. *GUFI, a program for measurement and evaluation of powder pattern*; Heidelberger Geowiss. Abh. 68; Heidelberg, 1993; ISBN 3-89257-067-1.
(9) Visser, J. W. *J. Appl. Crystallogr.* **1969**, *2*, 89−95.
(10) LeBail, A.; Duroy, H.; Fourquet, J. L. *Mater. Res. Bull.* **1988**, *23*, 447−452.
(11) Rodriguez-Carvajal, J. *Abstracts of the Satellite Meeting on Powder Diffraction of the XV Congress of the IUCr, Toulouse, France*, 1990; International Union of Crystallography: Chichester, U.K., 1990; p 127.
(12) Cascarano, G.; Favia, L.; Giacovazzo, C. *J. Appl. Crystallogr.* **1992**, *25*, 310−317.
(13) Von Dreele, R. B.; Larson, A. C. *Los Alamos Ntl. Lab. Rep. LAUR* **1990**, 86−748.
(14) Rietveld, H. M. *J. Appl. Crystallogr.* **1969**, *2*, 65−71.
(15) Thompson, P.; Cox, D. E.; Hastings, J. B. *J. Appl. Crystallogr.* **1987**, *20*, 79.
(16) Finger, L. W.; Cox, D. E.; Jephcoat, A. P. *J. Appl. Crystallogr.* **1994**, *27*, 892.
(17) Lightfoot, P.; Metha, M. A.; Bruce, P. G. *Science* **1993**, *262*, 883−885.
(18) Schenk, W. A. In *Experimental Organometallic Chemistry*; Wayda, A. L., Darensbourg, M. Y., Eds.; American Chemical Society: Washington, DC, 1987; pp 249−250.

was purged with dry chilled dinitrogen for at least 30 min prior to data collection. This purge continued throughout the experiments. Cell temperature varied from 80 to 100 K (by thermocouple) once cooling was well established.

Single-beam spectra of 1 cm^{-1} resolution were collected. For each sample a series of spectra were taken as the sample cooled. When no changes in the infrared spectrum were seen over a 20 min period, the cooling was considered complete and a final spectrum (an average of 64 transients) was acquired. The KBr pellets remained transmissive throughout the cooling as demonstrated by room-temperature spectra acquired after each low-temperature experiment.

Room-temperature data (cm^{-1}): ν(CO) 2023, 1971, 1957 vs, 1911 w; 1304 m; 1107, 1016 s; ρ(P−Me_2) 869 w. Low-temperature data: ν(CO) 2023, 1972, 1954 vs, 1910 w; 1306 m; 1108, 1016 s; ρ(P-Me_2) 871, 867 w.

Low-Temperature Differential Scanning Calorimetry. Measurements were made on a Perkin-Elmer DSC-2 configured for low-temperature operation, using liquid nitrogen as coolant. In a typical run 2−5 mg of $[Ru_2\{\mu_2{:}\mu_2{:}\eta^2\text{-}O_2PMe_2\}_2(CO)_4]_n$ was cooled to 180 K and then brought to 270 K at a rate of 10 K/min; at least two cooling−heating cycles were measured for each sample. Each cooling and heating cycle showed an endotherm between 210 and 230 K, but its intensity and exact onset temperature depended on sample history and the temperature program used.

Acknowledgment. We gratefully acknowledge financial support from the Brookhaven Visiting Scholars Program and the Henry and Camille Dreyfus Foundation for a Teacher-Scholar award (D.S.B.). We are grateful to Dick Harlow for helpful discussions on various aspects of the data analysis. Research carried out at the National Synchrotron Light Source at Brookhaven National Laboratories is supported by the U.S. Department of Energy, Division of Materials Sciences and Division of Chemical Sciences. The SUNY X3 Beamline at NSLS is supported by the Division of Basic Energy Sciences at the U.S. Department of Energy under Grant DE-FG02-86ER45231.

Supporting Information Available: Tables of positional parameters and observed and calculated structure factors for the low- and high-temperature phases of $[Ru_2\{\mu_2{:}\mu_2{:}\eta^2\text{-}O_2PMe_2\}_2(CO)_4]_n$ (35 pages). Ordering information is given on any current masthead page.

IC970265N